Supplemental Document

Intense optical parametric amplification in dispersion-engineered nanophotonic lithium niobate waveguides: supplement

LUIS LEDEZMA,[1,2,†] RYOTO SEKINE,[1,†] QIUSHI GUO,[1,†] RAJVEER NEHRA,[1] SAMAN JAHANI,[1] AND ALIREZA MARANDI[1,*]

[1] *Department of Electrical Engineering, California Institute of Technology, Pasadena, California 91125, USA*
[2] *Jet Propulsion Laboratory, California Institute of Technology, Pasadena, California 91109, USA*
[†] *These authors contributed equally to this work.*
[*] *Corresponding author: marandi@caltech.edu*

Supplement DOI: https://doi.org/10.6084/m9.figshare.19274822

Parent Article DOI: https://doi.org/10.1364/OPTICA.442332

Intense optical parametric amplification in dispersion-engineered nanophotonic lithium niobate waveguides: supplemental document

On this supplementary document, we include background theory on CW parametric amplification in waveguides as well as details on the nonlinear single envelope simulations for OPA and OPG. We also include additional fabrication and characterization details and a companion table for Fig. 4 of the main text.

1. CW PARAMETRIC AMPLIFICATION THEORY

We briefly review here the CW theory of degenerate parametric amplification, in which a strong pump field at frequency ω_p interacts with a signal field at frequency $\omega_s = \omega_p/2$. In the limit of no loss, the coupled wave equations are

$$\frac{\partial A_p}{\partial z} = -i\kappa A_s^2 e^{i\Delta k z}, \tag{S1}$$

$$\frac{\partial A_s}{\partial z} = -i\kappa A_s^* A_p e^{-i\Delta k z}, \tag{S2}$$

where A_p and A_s are the pump and signal complex envelopes, normalized such that $|A_i|^2$ is the power carried by the pulses, $\Delta k = \beta_p - 2\beta_s - 2\pi/\Lambda$ is the phase mismatch, and κ is the nonlinear coupling coefficient, which is related to the second harmonic normalized efficiency η by

$$\eta = \kappa^2 = \frac{2\omega_s^2 d_{\text{eff}}^2}{n_{\omega_s}^2 n_{\omega_p} \epsilon_0 c^3 A_{\text{eff}}}. \tag{S3}$$

Here, $d_{\text{eff}} = (2/\pi) d_{33}$ for periodic quasi-phase matching with 50% duty cycle, $d_{33} \approx 20.5$ pm/V for a pump centered at 1045 nm, and A_{eff} is the effective area of the nonlinear interaction, given by [1],

$$A_{\text{eff}} = \frac{\left(\int \left(\mathbf{e}_{\omega_s} \times \mathbf{h}_{\omega_s}^*\right) \cdot \mathbf{dS}\right)^2 \int \left(\mathbf{e}_{\omega_p} \times \mathbf{h}_{\omega_p}^*\right) \cdot \mathbf{dS}}{\left|\int \sum_{i,j,k} \bar{d}_{ijk} e_{i,\omega_p}^* e_{j,\omega_s} e_{k,\omega_s} dx dy\right|^2}, \tag{S4}$$

where $\mathbf{e}_\mu$ are dimensionless transverse mode profiles scaled such that the peak value of $\left(\mathbf{e}_\mu \times \mathbf{h}_\mu^*\right) \cdot \mathbf{z}$ is unity, and $\bar{d}_{ijk}$ is the $\chi^{(2)}$ tensor normalized with respect to d_{33}. Note that a large overlap integral (denominator of A_{eff}) leads to a small effective area and a stronger nonlinear interaction (large η).

Assuming no pump depletion, the signal equation of motion reduces to

$$\frac{\partial A_s}{\partial z} = -i\kappa A_p A_s^* e^{-i\Delta k z} = \gamma A_s^* e^{-i\Delta k z}, \tag{S5}$$

where $\gamma \equiv -i\kappa A_p$ can be made real by an appropriate definition of the pump absolute phase. This equation can be solved by separating the signal into its real and imaginary parts (i.e. its quadratures), $A_s = A_1 + iA_2$, yielding for the real part:

$$A_1(z) = A_1(0)\left[\cosh(gz) + \frac{\gamma}{g}\sinh(gz)\right]\exp(i\Delta k z/2) + A_2(0)\frac{\Delta k}{2g}\sinh(gz)\exp(i\Delta k z/2), \tag{S6}$$

where we have introduced the parametric gain parameter $g = \sqrt{|\gamma|^2 - (\Delta k/2)^2} = \sqrt{\eta P_p - (\Delta k/2)^2}$.

In the large gain regime, $\eta P_p \gg (\Delta k/2)^2$, $\gamma/g \approx 1$ and $\Delta k/2g \approx 0$, so the power of the real quadrature grows as

$$|A_1(z)|^2 = G|A_1(0)|^2 = |A_1(0)|^2 \exp(2gz) \approx |A_1(0)|^2 \exp\left(2\sqrt{\eta P_p} z\right), \tag{S7}$$

with a power gain $G \approx \exp\left(2\sqrt{\eta P_p} z\right)$.

For the case of non-degenerate operation, if only the pump and the signal are present at the input, then an idler will be generated with the right phase to produce signal amplification. In that case the amplification is not phase-sensitive and the gain is given by:

$$G = \frac{\gamma^2}{g^2} \sinh^2(gz), \tag{S8}$$

where g and γ are the same as in the degenerate case, but the phase mismatch is $\Delta k = \beta_p - \beta_s - \beta_i - 2\pi/\Lambda$. This gain expression was used to generate Fig. 3e on the main paper.

2. SINGLE ENVELOPE SIMULATION

We used a method similar to that described in [2] to simulate quadratic interactions over a large bandwidth using a single envelope in the frequency domain. We write a spectral component of the electric field propagating in the z-direction on a single waveguide mode as:

$$\mathbf{E}(x, y, \omega) = A(z, \Omega)\mathbf{e}(x, y, \omega) e^{-i(\beta_0 - \omega_0/v_{\text{ref}})z}, \tag{S9}$$

where ω and $\Omega = \omega - \omega_0$ are the optical and envelope angular frequencies, ω_0 is the simulation center frequency, β_0 is the waveguide propagation constant at ω_0, v_{ref} is the simulation reference frame velocity, x, y are the transversal waveguide coordinates, $\mathbf{e}(x, y, \omega)$ is the mode transversal field distribution, and $A(z, \omega)$ is the complex amplitude of the field that evolves during propagation. Note that $A(z, \omega)$ is a rapidly-varying envelope, i.e. it includes the phase factor $e^{-i\beta(\omega)z}$ acquired during linear propagation. Furthermore, $A(z, \omega)$ is an analytic signal, i.e., it only contains positive frequencies ($A(z, \omega < 0) = 0$).

We obtained an equation of motion for $A(z, \Omega)$ by ignoring counter-propagating terms (which are usually phase mismatched), and assuming a constant nonlinear coefficient and mode overlap integral, both of which are weak functions of frequency away from any material resonances. No limitations are placed upon the maximum spectral bandwidth of the simulation. The resulting propagation equation is,

$$\frac{\partial A}{\partial z} = -i\left[\beta(\omega) - \beta_0 - \frac{\Omega}{v_{\text{ref}}} - i\frac{\alpha}{2}\right] A - \frac{i\omega\epsilon_0 X_0}{8} d(z) \mathcal{F}_\Omega\left\{a^2(z,t) e^{j\phi(z,t)} + 2a(z,t)a^*(z,t) e^{-j\phi(z,t)}\right\}, \tag{S10}$$

where $d(z) = \pm 1$ is the sign of the quadratic nonlinear coefficient that is modulated in quasi-phase matching, $a(z, t)$ is the time domain representation of $A(z, \Omega)$, $\phi(z, t) = \omega_0 t - (\beta_0 - \omega_0/v_{\text{ref}})z$, $\mathcal{F}_\Omega$ is the Fourier transform in the Ω variable. The effective nonlinear coefficient X_0 is defined as:

$$X_0 = \sum_{ijk} \chi^{(2)}_{ijk} \int e^*_i(\omega_1) e_j(\omega_2) e_k(\omega_1 - \omega_2)\, \mathrm{d}S\,, \tag{S11}$$

where $\chi^{(2)}_{ijk}$ is the quadratic nonlinear susceptibility tensor, j, k, l are Cartesian components of the corresponding vectors, and ω_1 and ω_2 are two suitable chosen frequencies, e.g., the signal and pump frequencies in our case.

The time domain terms inside the Fourier transform of Eq. (S10) represent the processes of sum frequency generation ($\propto a(t)^2$) and difference frequency generation ($\propto a(t)a(t)^*$), which combined can predict all classical second order interactions, such as second harmonic generation and parametric amplification. Since $A(z)$ is fast varying, carrier dynamics can be resolved. In particular, phase mismatch is automatically included and the term $d(z)$ can be used to accurately simulate different quasi-phase matching gratings. This also means that the spatial domain needs to be sampled finely enough to resolve these dynamics. We solve the evolution equation (S10) with the split-step Fourier technique using the fourth-order Runge-Kutta method for the nonlinear step.

We used a combination of commercial software (Lumerical Inc.) and custom built effective-index routines to solve for the waveguide modes and generate the dispersion characteristics shown in Fig. 1c,d of the main text.

3. SMALL-SIGNAL OPA SIMULATION

We simulated optical parametric amplification for the dispersion-engineered 2.5-mm-long waveguide described in the main text, including quasi-phase matching through a periodic modulation of $d(z)$. As the input, we used a 100-fs-long pump pulse centered at 1045 nm, and a 35-fs-long signal pulse centered at 2090 nm, both with a hyperbolic secant profile. The output power spectral density (PSD) for three pump power levels, with a fixed input signal level, are shown in Fig. S1a. For the largest pump pulse energy shown, significant spectral broadening is observed at both, the pump and signal wavelengths, revealing a strong non-linear regime similar to [1]. Figure S1b shows the gain as a function of the pump energy for three different input signal levels as well as the CW theory and measured data. Pump depletion and spectral broadening effects make the gain deviate from the theoretical CW prediction at large pump and signal power levels (to calculate the gain, the output signal energy is integrated from 1,600 nm to 3,000 nm). At low pump power levels, the pulsed gain curve follows the CW theory as expected for dispersion-engineered waveguides according to the argument provided in the main paper. Note that a low signal level is necessary in order to extract the maximum gain from a strong pump. It is for this reason that to characterize the maximum gain of our waveguides we performed measurements on the OPG regime, with no input signal except for vacuum fluctuations.

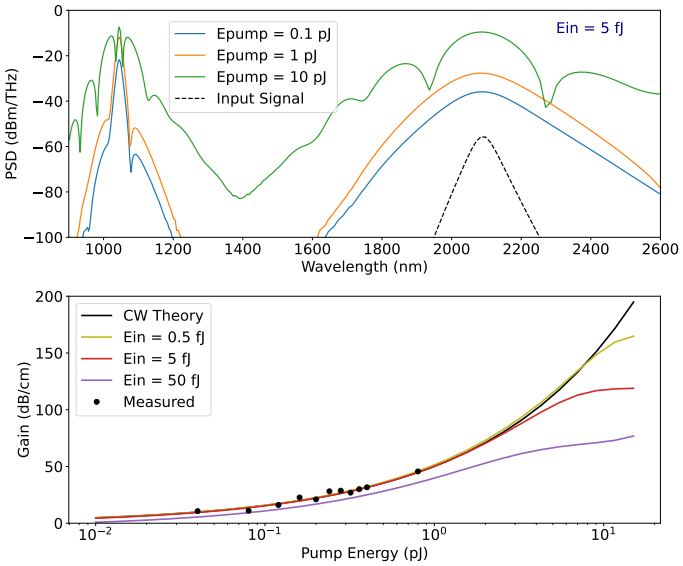

Fig. S1. Numerical simulation of small-signal optical parametric amplification. a, Power spectral density at the output of a 2.5-mm-long, dispersion-engineered waveguide showing low distortion parametric amplification for pump energies of 0.1 pJ and 1 pJ, and spectral broadening for a pump energy of 10 pJ. The 100-fs-long pump is centered at 1045 nm and the 35-fs-long signal is centered at 2090 nm. The input signal energy is fixed at 5 fJ. **b**, Simulated gain as a function of pump power for three different input signal levels along with the prediction from the CW theory and the measured values (from main paper Fig. 2c). It is evident that the CW theory is valid for this dispersion-engineered waveguide before gain saturation and spectral broadening effects start dominating at high pump power levels. The maximum measured gain was limited by input coupling losses, and improving the input coupling by 10 dB leads to small-signal gains exceeding 150 dB/cm, putting the on-chip OPA in direct competition with the largest single mode SOA gains reported.

4. OPG SIMULATION

In the main text we argue that operating the amplifier in the OPG regime (with a strong pump and no input signal) provides a practical way of extracting the gain of the amplifier avoiding saturation effects and also revealing its full gain-bandwidth. In this section we support these claims with semi-classical simulations of parametric generation.

Seeding the OPA with an input noise having an energy of half-a-photon per frequency mode, and a uniformly distributed random phase, has been known to provide the same average signal output power as the quantum mechanical solution [3]. This is equivalent to neglecting thermal excitations and modeling the remaining vacuum fluctuations as complex Gaussian random variables with zero mean and a half-a-photon variance [4]. Fig. S2a shows the simulated average output power (integrated from 1,600 nm to 3,000 nm) for the 6-mm-long dispersion-engineered waveguide, along with the expected curve from the CW theory and our measured data. The simulation deviates from the theory at pump energies larger than 4 pJ due to efficient parametric generation (OPG) producing pump depletion (also shown in Fig. S2a). The simulations results shown in Fig. S2a are the ensemble average of 100 simulations, each simulation producing a different result due to the stochastic nature of the input signal. This is illustrated in Fig. S2b., where the output spectra OPG for a pump energy of 3 pJ is shown for the first 20 simulations along with the average of 100 simulations.

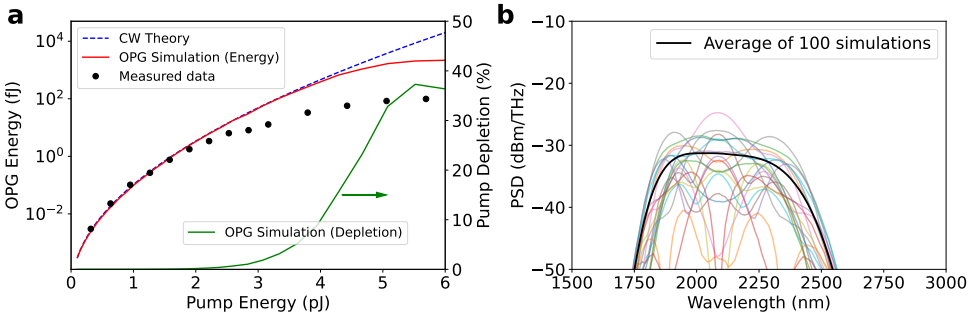

Fig. S2. Numerical simulation of optical parametric generation. a, Simulated OPG energy as a function of pump energy along with the CW theory and measured data. The pump is a 100-fs-long hyperbolic secant pulse center at 1045 nm. The results are the average of 100 simulations. In each simulation, the input signal is a realization of a complex Gaussian random variable with zero mean and half-a-photon variance. The simulation results deviate from the CW theory for pump energy levels above ~4 pJ beyond which efficient parametric generation occurs and the no-pump-depletion approximation is no longer valid. The simulated pump depletion level ($P_{\mathrm{OPG}}/P_{\mathrm{pump}}$) is shown on the right hand axis. **b**, Output power spectral density for 20 OPG simulations illustrating its stochastic nature, as well as the average for 100 simulations.

5. DEVICE FABRICATION

We used a commercial wafer (NANOLN), with a 700-nm-thick X-cut MgO-doped LN thin-film on 2-μm-thick SiO_2. The fabrication process begins with periodically poling the chip. The poling electrodes (15 nm Cr/55 nm Au) were patterned using e-beam lithography, e-beam evaporation and metal lift-off. Then ~300 V pulses were applied across the electrodes to produce periodic domain inversion over a 6-mm length with a period of ~5 μm. We visually inspected the poling quality using second harmonic microscopy (an example image is shown in an inset of Fig. 2a. The metal electrodes were removed by chemical etching. The waveguides were patterned by e-beam lithography using hydrogen silsesquioxane (HSQ) as the e-beam resist. The pattern was transferred to the LN layer by dry etching with Ar^+ plasma. Finally, the waveguide facets were polished to reduce the coupling losses.

6. DISPERSION ENGINEERING MAPS

After selecting a thin-film thickness of 700 nm, the width and etch depth of the waveguide can be varied to create maps of GVD at 2 μm and GVM between the 1 μm pump and 2 μm signal. We can also factor-in the waveguide length and pulse width by the following procedure. The GVM between the signal and pump defines a walk-off length given by $L_{\mathrm{gvm}} = \tau/\mathrm{GVM}$, where τ is the pulse width. If the waveguide width is L_{wg}, then we want to minimize the ratio $L_{\mathrm{wg}}/L_{\mathrm{gvm}}$. A map of this ratio, for $L_{\mathrm{wg}} = 6$ mm and $\tau = 35$ fs, is shown in Fig. S3a, along with the corresponding contour levels at 0.5 (where the waveguide is half the walk-off length).

Similarly, a dispersion length can be defined as $L_{\mathrm{gvd}} = \tau^2/\mathrm{GVD}$, and the metric would be the ratio $L_{\mathrm{wg}}/L_{\mathrm{gvd}}$. The corresponding map is shown in Fig. S3b, along with the contour level at 0.25 (where the waveguide is only a quarter of the dispersion length). For both contours in Fig. S3, the black dot corresponds to our waveguide geometry.

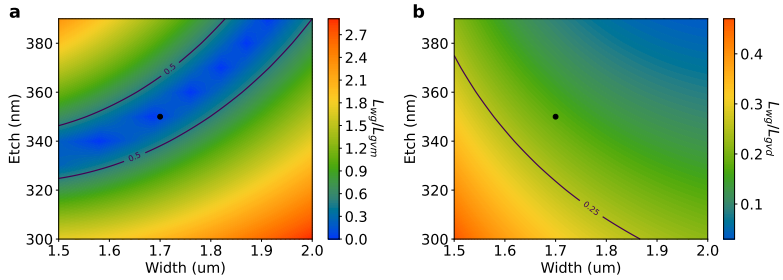

Fig. S3. Dispersion engineering mappings. a, Waveguide length to walk-off length ratio. **b**, Waveguide length to dispersion length ratio. Both maps are for a 700-nm thick film, 6-mm long waveguide, and 35-fs pulse width. The black dot indicates our waveguide design.

7. WAVEGUIDE CHARACTERIZATION

For the OPA measurements we use the setup shown in Fig. 2a with both, 1 μm and 2 μm pulses, coupled into the waveguide. The 1 μm source (the pump) was a 1 W Yb mode-locked laser that produces nearly transform-limited 75-fs-long pulses at a 250 MHz repetition rate (Menlo Systems Orange). Part of the pump was sent directly to the chip, while the rest was fed into a near-synchronously pumped degenerate OPO [5] to produce 2 μm pulses. The 1 μm and 2 μm pulses were combined at a dichroic mirror, and coupled into the waveguides using a reflective objective (Newport 50102-02). The two pulses were temporally overlapped by adjusting the optical delay line, and their relative phase was scanned by the piezoelectric transducer on the delay line. The chip was placed on a thermoelectric cooling stage (TEC), and the temperature was finely tuned to adjust the quasi-phase matching condition. The output of the chip was collected with another reflective objective and the remaining pump power was filtered. A 2 μm detector followed by an oscilloscope was used to monitor the entire signal power without and without the pump beam (Fig. 2b). We used an optical spectrum analyzer (OSA) covering 1200 - 2400 nm (Yokogawa AQ6375B) with a 2 nm resolution bandwidth (Fig. 2c) to characterize the spectral gain distribution.

For the OPG measurements of Fig. 3 of the main text, only the 1 μm path was used. The output of a 10-W Yb mode-locked laser (Menlo Systems Orange High Power 10) with 100-fs pulse length was passed through an optical chopper to reduce thermally induced damage. The average input power was swept using a variable ND filter and the output was recorded using the same OSA.

The input/output coupling losses were estimated based on a combination of linear and nonlinear measurements as follows. Comparing the optical power before and after the chip gives the total loss $L_t = L_i + L_{wg} + L_o$, where L_i is the input coupling loss, L_{wg} is the waveguide loss, and L_o is the output coupling loss. We estimated the waveguide loss, L_{wg}, to be much less than 1 dB based on Q-factor measurements in other chips using the same fabrication process. Since the total loss L_t is ~29 dB (at 2 μm) we neglect the waveguide loss in what follows.

As explained in Section 3B of the main article, the OPG data can be used to estimate the gain $G_s = \exp(2gL)$ without any knowledge of the input/output coefficients. This is because this gain depends only on the rate of growth of the OPG power, and not on its absolute value. We also know that the expected number of photons generated during OPG is given by $\langle n \rangle = \sinh^2(gL) \approx 0.25 \exp(2gL) = 0.25 G_s$. Thus, by estimating G_s, we are also estimating the average number of photons generated, from which the OPG power in the waveguide follows immediately: $P_{\mathrm{OPG}} = \hbar\omega \langle n \rangle f_{rep}$. Comparing this expected power with the measured power gives us a total output collection efficiency of 5.85 dB at 2 μm. This corresponds to 26 % output coupling efficiency, which compares well with output coupling losses in similar waveguides estimated by other methods [6].

Subtracting this output coupling loss from the total throughput loss gives us an input coupling loss at 2 μm of ~23 dB, which is considerably larger than the output coupling loss. This is expected

Table S1. Comparison of on-chip amplifiers gain and bandwidth

Type	Length	Gain		Signal	3-dB Bandwidth (Signal + Idler)		Reference
		Absolute	Normalized	Wavelength	Absolute	Relative	
$\chi^{(2)}$	6 mm	62 dB	104 dB/cm	2090 nm	380 nm (26 THz)	18.2 %	This Work
$\chi^{(2)}$	12 mm	100 dB	83 dB/cm	2700 nm	10 nm (1.64 THz)	0.4 %	[7]
SOA	1.2 mm	25.5 dB	213 dB/cm	1575 nm	34 nm (4.11 THz)	2.2 %	[8]
SOA	2 mm	13 dB	65 dB/cm	2010 nm	75 nm (5.6 THz)	3.7 %	[9]
SOA	2 mm	25 dB	125 dB/cm	1550 nm	69 nm (8.1 THz)	4.5 %	[10]
FWM $\chi^{(3)}$	4 mm	25.4 dB	63.5 dB/cm	2170 nm	50 nm (3.18 THz)	2.3 %	[11]
FWM $\chi^{(3)}$	2 cm	45 dB	22.5 dB/cm	2170 nm	150 nm (9.5 THz)	6.9 %	[12]
FWM $\chi^{(3)}$	1.7 cm	13.9 dB	8.2 dB/cm	1550 nm	40 nm (5 THz)	2.7 %	[13]
SBS	2.9 cm	5.2 dB	1.8 dB/cm	1550 nm	< 50 MHz	$\ll$ 0.1 %	[14]
SRS	4.6 cm	2.3dB dB	0.5 dB/cm	1545 nm	80 GHz	< 0.1 %	[15]
Er^{+} doped	3.6 cm	18 dB	5 dB/cm	1530 nm	20 nm (2.56 THz)	1.3 %	[16]
$C\chi^{(2)}$	2 cm	38.3 dB	19.2 dB/cm	1550 nm	+14 THz	7.2 %	[17]

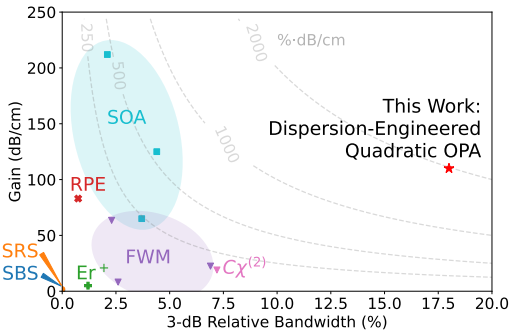

Fig. S4. Comparison of the gain and bandwidth of quadratic OPA in dispersion-engineered LN waveguides with other gain mechanisms in integrated photonics. This is an alternative representation of the data in Fig. 4 of the main text using relative bandwidth as the horizontal axis.

since only the power coupled to the fundamental TE mode is considered at the input, while most of the radiated modes are expected to be collected by the objective at the output. At 1 μm, we assume that the output coupling loss is also 5.85 dB, since we use a low-dispersion metallic collective objective. The measured throughput loss at 1 μm is ~31 dB, so the input coupling loss was estimated to be ~25 dB. Note that the input coupling loss at 1 μm is expected to be larger than that at 2 μm due to the corresponding mode sizes.

8. ON-CHIP AMPLIFIER STATE OF THE ART COMPARISON

Detailed bandwidth and gain numbers used to generate Fig. 4 from the main text and Fig. S3 are available in Table S1 along with the corresponding references. Previous works include only on-chip traveling-wave amplifiers. We have striven to include the best and most recent results, but not all publications report enough data to extract 3 dB bandwidth values and couldn't be added to the comparison. To estimate the bandwidth of the FWM cases we have added together the signal and idler bandwidths.

REFERENCES

1. M. Jankowski, C. Langrock, B. Desiatov, A. Marandi, C. Wang, M. Zhang, C. R. Phillips, M. Lončar, and M. M. Fejer, "Ultrabroadband nonlinear optics in nanophotonic periodically poled lithium niobate waveguides," Optica **7**, 40–46 (2020).

2. C. R. Phillips, C. Langrock, J. S. Pelc, M. M. Fejer, I. Hartl, and M. E. Fermann, "Supercontinuum generation in quasi-phasematched waveguides," Opt. Express **19**, 18754–18773 (2011).
3. D. A. Kleinman, "Theory of Optical Parametric Noise," Phys. Rev. **174**, 1027–1041 (1968).
4. G. Arisholm, "Quantum noise initiation and macroscopic fluctuations in optical parametric oscillators," J. Opt. Soc. Am. B **16**, 117 (1999).
5. M. Jankowski, A. Marandi, C. R. Phillips, R. Hamerly, K. A. Ingold, R. L. Byer, and M. M. Fejer, "Temporal simultons in optical parametric oscillators," Phys. Rev. Lett. **120**, 053904 (2018).
6. M. Jankowski, N. Jornod, C. Langrock, B. Desiatov, A. Marandi, M. Lončar, and M. M. Fejer, "Efficient Octave-Spanning Parametric Down-Conversion at the Picojoule Level," arXiv:2104.07928 [physics] (2021). ArXiv: 2104.07928.
7. X. Xie, A. M. Schober, C. Langrock, R. V. Roussev, J. R. Kurz, and M. M. Fejer, "Picojoule threshold, picosecond optical parametric generation in reverse proton-exchanged lithium niobate waveguides," JOSA B **21**, 1397–1402 (2004).
8. K. V. Gasse, R. Wang, and G. Roelkens, "27 dB gain III–V-on-silicon semiconductor optical amplifier with > 17 dBm output power," Opt. Express **27**, 293–302 (2019).
9. N. Volet, A. Spott, E. J. Stanton, M. L. Davenport, L. Chang, J. D. Peters, T. C. Briles, I. Vurgaftman, J. R. Meyer, and J. E. Bowers, "Semiconductor optical amplifiers at 2.0-µm wavelength on silicon," Laser & Photonics Rev. **11**, 1600165 (2017).
10. M. L. Davenport, S. Skendžić, N. Volet, J. C. Hulme, M. J. R. Heck, and J. E. Bowers, "Heterogeneous Silicon/III–V Semiconductor Optical Amplifiers," IEEE J. Sel. Top. Quantum Electron. **22**, 78–88 (2016).
11. X. Liu, R. M. Osgood, Y. A. Vlasov, and W. M. J. Green, "Mid-infrared optical parametric amplifier using silicon nanophotonic waveguides," Nat. Photonics **4**, 557–560 (2010).
12. B. Kuyken, X. Liu, G. Roelkens, R. Baets, J. Richard M. Osgood, and W. M. J. Green, "50 dB parametric on-chip gain in silicon photonic wires," Opt. Lett. **36**, 4401–4403 (2011).
13. M. A. Foster, A. C. Turner, J. E. Sharping, B. S. Schmidt, M. Lipson, and A. L. Gaeta, "Broadband optical parametric gain on a silicon photonic chip," Nature **441**, 960–963 (2006).
14. E. A. Kittlaus, H. Shin, and P. T. Rakich, "Large Brillouin amplification in silicon," Nat. Photonics **10**, 463–467 (2016).
15. V. Sih, S. Xu, Y.-H. Kuo, H. Rong, M. Paniccia, O. Cohen, and O. Raday, "Raman amplification of 40 Gb/s data in low-loss silicon waveguides," Opt. Express **15**, 357–362 (2007).
16. J. Zhou, Y. Liang, Z. Liu, W. Chu, H. Zhang, D. Yin, Z. Fang, R. Wu, J. Zhang, W. Chen, Z. Wang, Y. Zhou, M. Wang, and Y. Cheng, "On-chip integrated waveguide amplifiers on Erbium-doped thin film lithium niobate on insulator," arXiv:2101.00783 [physics] (2021).
17. Y. M. Sua, J.-Y. Chen, and Y.-P. Huang, "Ultra-wideband and high-gain parametric amplification in telecom wavelengths with an optimally mode-matched PPLN waveguide," Opt. Lett. **43**, 2965–2968 (2018). Publisher: Optical Society of America.